17th World Conference on Earthquake Engineering, 17WCEE
Sendai, Japan - September 13th to 18th 2020

Investigation of lateral viscous boundary in two-phase dynamic analysis of 3D irregular layer system ground

K. Kaneda(1)

(1) *Chief Researcher, Takenaka Research & Development Institute, kaneda.kazuhiro@takenaka.co.jp*

Abstract

When performing soil dynamic analysis, viscous boundary connecting the free field and repeated boundary are often used as lateral boundary conditions. Eventually, traction force on the lateral boundary considering both soil and water was introduced. Analysis with proposed traction force was then performed to analyze a relatively small boundary, thereby showing results similar to a sufficiently large boundary. This paper aims to investigate the influence of traction force and to propose a viscous boundary in a two-layer system. In the horizontal direction, a viscous boundary was installed, which required traction force. Its two-phase formulation was conducted to simulate a 3D irregular ground. Irregular soil layer in both z- and y- directions was constructed. With traction force considered and not, clearly different responses were exhibited. Considering traction force negligible, the response of the building was affected. However, considering the viscous boundary, these responses were almost the same, thereby showing that it can be analyzed with a relatively small boundary.

Keywords: Lateral Viscous Boundary, Dynamic Analysis, Traction Force

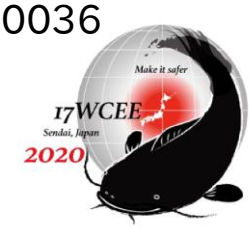

1. Introduction

When performing soil dynamic analysis, viscous boundary connecting the free field and repeated boundary are often used as lateral boundary conditions. However, in a 3D analysis of an irregular soil layer or tetrahedral element, the free ground on the side differs on all four outside fields and various measures are needed to reduce the influence of reflected waves from the free field. Among these measures are to consider the traction force of the lateral free ground [1, 2] and to formulate a two-phase analysis. In liquefaction analysis, a two-phase analysis of soil and water is performed. uU formulation [3] is used to solve the equations for water and soil motion and up formulation is used to formulate soil skeleton displacement and water pressure. Moreover, different boundaries should be handled. In this research, two-phase analysis is conducted using uU Formulation. The lateral viscous boundary formulation considering soil and water traction force for higher-order elements, such as tetrahedral elements, was also discussed. A dynamic 3D analysis with irregular soil layers was performed with its accuracy examined.

2. Formulation of traction force applied to soil model side

The traction force at the side boundary that must be considered in seismic response analysis is the surface force acting on the vertical section of the infinite horizontal soil (free ground). This surface force vertically acts when horizontal ground motions are applied and horizontally acts when vertical ground motions are applied. It is equal to the reaction force when the displacement is restrained. In this study, the traction force is calculated from the surface force. Eq. (1) is a uU Formulation that discretizes the two-phase governing equation of the soil skeleton and pore water shown by Zienkiewicz and Shiomi [3] and adds the boundary surface force.

$$\int_{\Omega} \mathbf{B}^T \boldsymbol{\sigma} d\Omega + \mathbf{K_1 u} + \mathbf{K_2 U} - \mathbf{C_2 \dot{U}} + \mathbf{C_1 \dot{u}} + \mathbf{M^s \ddot{u}} - \int_{S} \mathbf{N}^T \boldsymbol{t}^s dS = \mathbf{f^s}$$

$$\mathbf{K_2^T u} + \mathbf{K_3 U} - \mathbf{C_2^T \dot{u}} + \mathbf{C_3 \dot{U}} + \mathbf{M^f \ddot{U}} - \int_{S} \mathbf{N}^T \boldsymbol{t}^f dS = \mathbf{f^f} \tag{1}$$

Where ***B***: strain displacement relation matrix, ***σ***: stress matrix, ***K***: stiffness matrix, ***C***: damping matrix, ***M***: mass matrix, *u*: displacement of soil skeleton, *U*: displacement of pore water, *f*: external force, ***t***: boundary surface force, (•) indicates time derivative. Superscripts *s* and *f* denote soil skeleton and pore water, respectively. The surface force of the vertical section of the free ground is obtained from the free ground stress by Eq. (2).

$$\mathbf{t_e} = \boldsymbol{\sigma}_\mathbf{e}^T \ \mathbf{n} \tag{2}$$

where $\boldsymbol{\sigma}_e$: stress matrix on the free ground (value that balances with the seismic load), **n**: normal vector of the boundary, $\boldsymbol{t}_e$: surface force of the boundary. In this study, the side viscous boundary element defines the element coordinate system for the boundary surface as shown in Fig. 1. In the element coordinate system, the outward normal direction of the boundary is z', the vertically upward direction is y', and the direction orthogonal to the plane formed by y 'and z' is x'. Assuming that the vertical upward direction of the global coordinate system is Z, y 'and Z are the same direction.

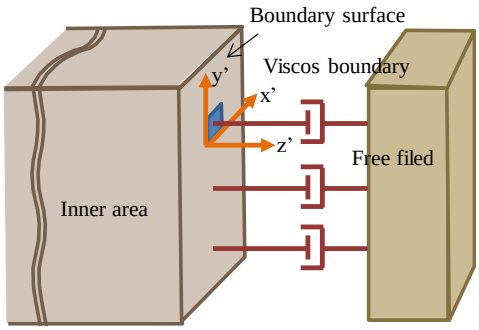

Fig. 1 Definition of the coordinates of the boundary surface

The z 'direction and direction of $\boldsymbol{n}$ are the same. In the element coordinate system, the surface force of Eq. (2) is expressed by Eq. (3).

$$\{t_{x'} \quad t_{y'} \quad t_{z'}\}^T = \{\tau_{z'x'} \quad \tau_{z'y'} \quad \sigma_{z'}\}^T \tag{3}$$

The equivalent nodal force due to the surface force is calculated by dividing the area acted on the traction force by Eq. (4). The element shape is arbitrary and can support higher-order elements.

$$\mathbf{f}_e' = \int_S \mathbf{N}^T \mathbf{t}_e dS \tag{4}$$

where $\boldsymbol{f_e}'$: equivalent nodal force in the element coordinate system.

Eq. (5) converts the equivalent nodal force from the element coordinate system to the global coordinate system.

$$\mathbf{f}_e = \mathbf{T}^T \mathbf{f}_e' \tag{5}$$

where $\boldsymbol{T}^T$: coordinate transformation matrix.

Since the traction force is obtained by converting the free field stress into a surface force, a stiffness matrix is not required. On the other hand, when assembling the whole stiffness matrix, the element stiffness matrix for the side viscous boundary elements should be constructed. The element stiffness matrix $\boldsymbol{K_e}'$ in the element coordinate system is as follows.

$$\mathbf{K}_e' = \int_S \mathbf{N}^T \mathbf{D}\mathbf{B} dS \tag{6}$$

$$\mathbf{D} = \begin{bmatrix} 0 & 0 & D_{z'x'} & 0 \\ 0 & 0 & 0 & D_{z'y'} \\ D_{x'x'} & D_{y'y'} & 0 & 0 \end{bmatrix} \tag{7}$$

$$\mathbf{B} = \begin{bmatrix} \frac{\partial N_i}{\partial x'} & 0 & 0 \\ 0 & \frac{\partial N_i}{\partial y'} & 0 \\ 0 & 0 & \frac{\partial N_i}{\partial x'} \\ 0 & 0 & \frac{\partial N_i}{\partial y'} \end{bmatrix} \tag{8}$$

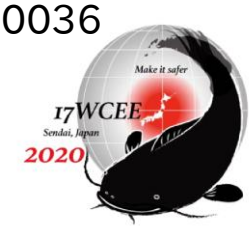

To obtain the element stiffness determinant (9) in the global coordinate system, the element stiffness determinant (6) is multiplied by the coordinate transformation matrix. Here, $D_{x'x'}$ represents the component of D and N as a shape function.

$$\mathbf{K}_e = \mathbf{T}^T \mathbf{K}_\mathbf{e}' \mathbf{T} \tag{9}$$

Eq. (9) is defined in the coupled term between free field and boundary.

$$\mathbf{K} = \begin{bmatrix} 0 & \mathbf{K}_e \\ 0 & 0 \end{bmatrix} \tag{10}$$

As shown in Eq. (10), the element stiffness matrix is asymmetric. If the stiffness matrix is symmetric, the force obtained from the displacement on the boundary side of the internal region acts on the free field side and Eq. (10) then becomes Eq. (11). This force should be essentially zero. However, the large mass of the free field makes the influence from the boundary negligible.

$$\mathbf{K} = \begin{bmatrix} 0 & \mathbf{K}_e \\ \mathbf{K}_e^T & 0 \end{bmatrix} \tag{11}$$

On the other hand, the formulation of pore water is as follows.

$$\mathbf{t_e} = \mathbf{n}p \tag{12}$$

where p is the excess pore water pressure.

$$p = -\mathrm{Q}\left(nU_{i,i} + (\alpha - n)u_{i,i}\right) \tag{13}$$

Q and a are

$$1/Q = n/K_f + (\alpha - n)/K_s \tag{14}$$

$$\alpha = 1 - K_T/K_s \tag{15}$$

where K_T, K_s, and K_f are the bulk modulus of the soil skeleton, soil particles, and pore water, respectively.

The surface force for water pressure is as follows.

$$\begin{Bmatrix} t^s \\ t^f \end{Bmatrix} = \begin{Bmatrix} -(\alpha - n)p \\ -np \end{Bmatrix} \tag{16}$$

Where t^s and t^f are the surface forces of the soil and water relative to the pore water pressure, respectively. The transformation from the element coordinate system to the global coordinate system is similar to that of Eq. (5). Next, the element stiffness matrices K_e^s, K_e^f, and K_e^{sf} for the soil skeleton, pore water, and soil-water coupling in the elemental coordinate system, respectively, are obtained following Eq. (17) to (19). Their equation expansion from the element stiffness matrix to the whole stiffness matrix is similar to Eq. (9) to (11).

$$\mathbf{K}_\mathrm{e}^s = -(\alpha - n)^2 \int_S \mathbf{N^T D^f B}\, dS \tag{17}$$

$$\mathbf{K}_\mathrm{e}^f = -n^2 \int_S \mathbf{N^T D^f B}\, dS \tag{18}$$

$$\mathbf{K}_{\mathrm{e}}^{sf} = -(\alpha - n)n \int_S \mathbf{N}^{\mathrm{T}} \mathbf{D}^{\mathrm{f}} \mathbf{B}\, dS \tag{19}$$

$$\mathbf{D}^{f} = \begin{bmatrix} 0 & 0 & 0 & 0 \\ 0 & 0 & 0 & 0 \\ Q & Q & 0 & 0 \end{bmatrix} \tag{20}$$

3. Analysis conditions

3.1 Analysis mesh

Figure 2 shows the analysis mesh with higher elements (10-node tetrahedron and 15-node pentahedron). An inclined ground is assumed for the embankment structures. In mesh (a), there is a large analysis area in the horizontal direction and free ground with sufficiently large mass connected to both sides to consider the influence of the wave propagation boundary. In mesh (b), there is a smaller analysis area and viscous boundaries connected to both sides. In mesh (c) there is a 10-meter extension of mesh (b) on all sides with the same layer. Table 1 shows the material constants used in the analysis. Impulse waves were input to the lower part of the ground. The transfer function with the upper center of the embankment marked red point in the Fig. 2 was then examined. The ground is first subjected to single-phase and two-phase analysis as linear analysis followed by liquefaction analysis using seismic waves as the non-linear analysis.

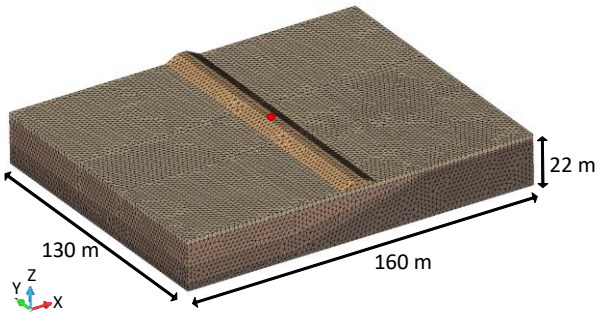

(a) Large mesh

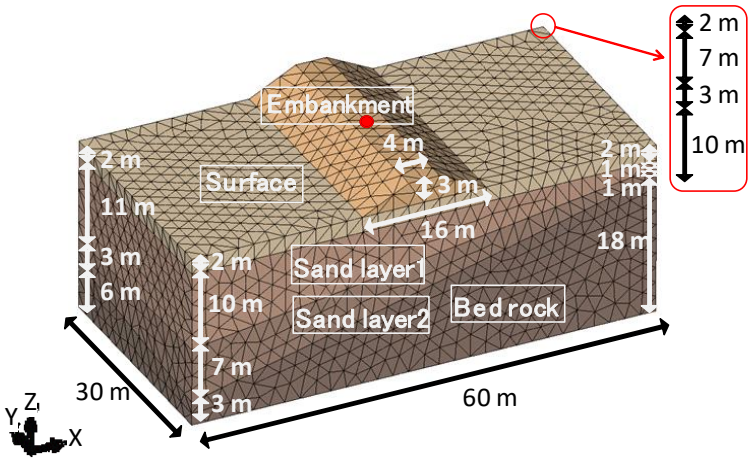

(b) Small mesh

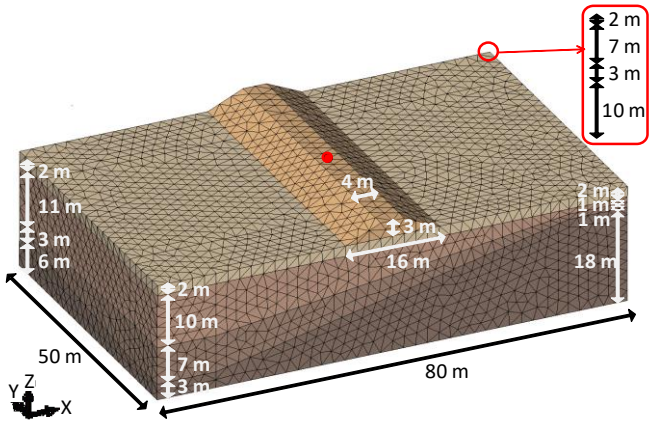

(c) Mesh obtained by extending a small mesh by 10 m in all directions

Fig. 2 Analysis meshes used in his study

Table 1 Material constants

	Embankment	Surface	Sand layer 1	Sand layer 2	Bed rock
Density of soil particle ρ_s (Mg/m^3)	—	—	2.65	—	2.65
Density of water ρ_f (Mg/m^3)	—	—	1.0	—	1.0
Porosity n	—	—	0.4081	—	0.3939
Wet density ρ (Mg/m^3)	1.8	1.98	1.98	1.98	
Shear stiffness G (kPa)	45000	112600	112600	112600	180000
Reffernce stress σ_{ref} (kPa)	18.0	49.0	49.0	49.0	—
Coefficient of restraint pressure dependent n	0.5	0.5	0.5	0.5	—
Poisson ratio ν	0.33	0.33	0.33	0.48	0.48
Cohesion c (kPa)	10.0	10.0	10.0	10.0	—
Shear resistance angle ϕ (deg.)	36.0	36.0	36.0	36.0	—
Soil particle bulk modulus K_s =1.0×10^{41} (kPa), Water bulk modulus K_f =2.2×10^6 (kPa), Permeability k =1×10^{-8} (m/s)					

3.2 Viscous boundary model

In the case of a 3D model with a viscous boundary shown in Fig. 3, free grounds were created on all sides of the mesh in Fig. 2 with the same shape as the boundary. Corner free grounds between the sides were also set. The mass of the side free ground was 10^3 times the mass of the inner area and that of the corner free ground was 10^6 times the mass of the inner area.

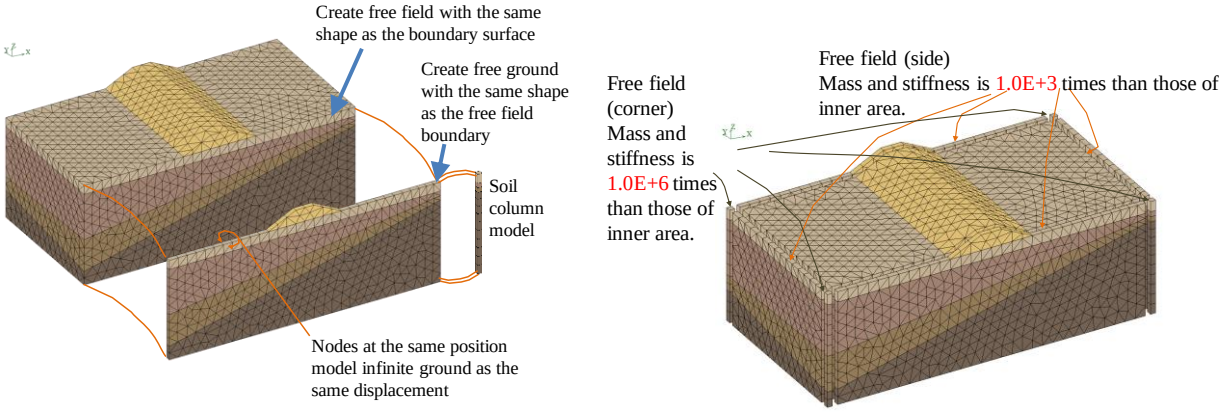

Fig. 3 3D model with viscous boundary

4. Analysis results: Impulse response

4.1 Single-phase analysis, linear response for ground

a) Comparison of viscous boundaries and rigidly connected internal area and free ground

In a rigid connection (tied), the nodes at the same position in the internal area and free ground have the same displacement. Fig. 4(a) and 4(b) show the transfer function of the analysis result of Fig. 2(a) and 2(b) mesh, respectively. This is the Fourier spectrum ratio of the response acceleration at the center of the embankment top (red point in Fig. 2(a)) for the input wave. Input motion is only in the X-direction for all analyses. In the case of a relatively large mesh in Fig. 4(a), a slight difference is observed around 7 Hz, however, both results are nearly similar. On the other hand, as shown in Fig. 4(b), the viscous boundary and rigid connection response differed greatly at around 10 Hz. Thus, with relatively larger mesh, there is minimal effect on its surrounding free ground even with a rigid connection.

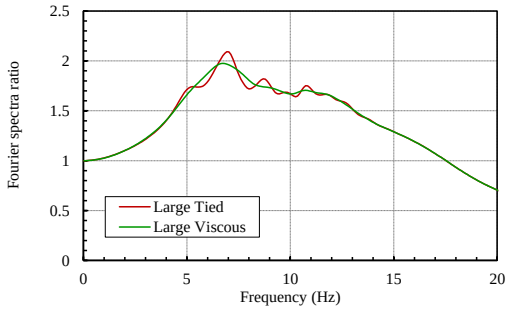

(a) Fig. 2(a) mesh

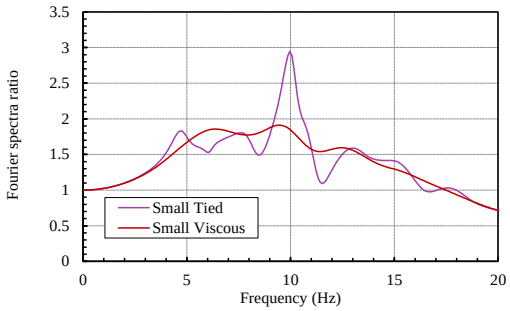

(b) Fig. 2(b) mesh

Fig. 4 Transfer function response from single -phase analysis

b) Internal area and free ground connected with a viscous boundary

Figure 5 shows the transfer function obtained from calculations to compare the differences between a large mesh (Fig. 2 (a)) and small mesh (Fig. 2 (b)) with viscous boundaries. The response of the small and large meshes tend to be equivalent, if not completely identical.

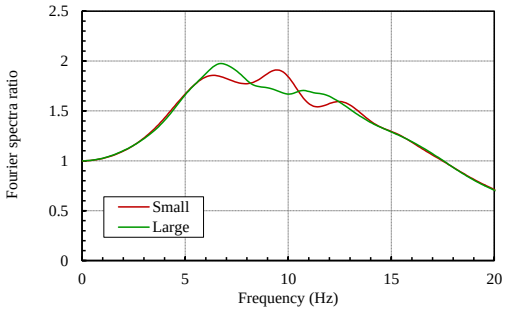

Fig. 5 Transfer function response of a large and small mesh with viscous boundaries using single-phase analysis

c) Traction force

Figure 6 shows a comparison when traction force is not considered (No traction) and when traction force is considered (Cal. Traction). The behavior significantly differed at 1 and 10 Hz for both cases. Therefore, traction force should be considered to discuss the surface response with a viscous boundary.

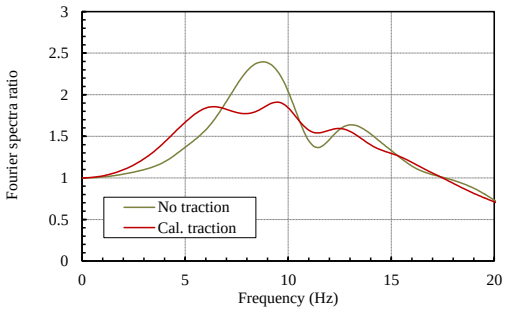

Fig. 6 Transfer function response with traction force considered and not using single-phase analysis

4.2 Two-phase analysis, linear response for ground

a) Internal area and free ground connected by viscous boundaries

In the two-phase analysis, the response tendency did not differ much from the single-phase analysis. Figure 7 shows the transfer function of the analysis result. Comparing the mesh connected at the viscous boundary of a large mesh (Fig. 2 (a)) and small mesh (Fig. 2 (b)), minimal differences can be observed.

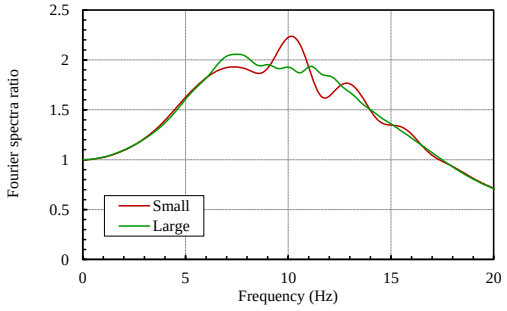

Fig. 7 Transfer function response of large and small mesh connected at a viscous boundary using two-phase analysis

b) Shear stiffness of liquefied layer and non-liquefied layer

From Section 4.1, a relatively good solution can be obtained for both single-phase and two-phase analysis by analyzing with a small mesh and viscous boundary while considering the traction force. Therefore, in liquefication analysis, the ground stiffness could be extremely reduced. Here, the shear stiffness of the liquefied layer was set at 1/10 and that of a non-liquified layer was set at 1/2 of the original shear stiffness. Figure 8 shows their transfer function result. There is no significant difference when analyzing with a small mesh and large mesh. The mesh of Fig. 2(b) has its viscous boundary set near the area with oblique soil. In Fig. 2(a), several meters of stratified ground is provided where the stratum and viscous boundary is set. Therefore, a similar analysis was performed on the 10-m stratified ground from a small mesh in Fig. 2(c). Figure 9 shows the analytical results. The difference between large mesh and small mesh is smaller than in Fig. 8. Therefore, the number of meshes should be reduced in performing 3D analysis. However, meshes are more accurate with a slightly stratified ground formed from a diagonal ground.

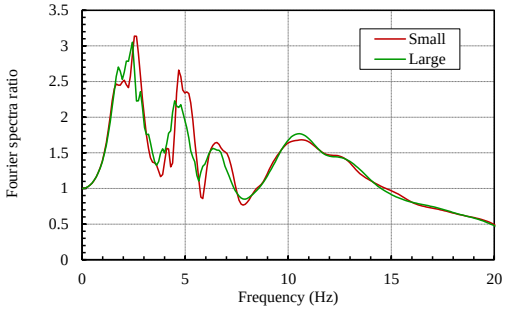

Fig. 8 Transfer function response of liquefied and non-liquefied layers using two-phase analysis

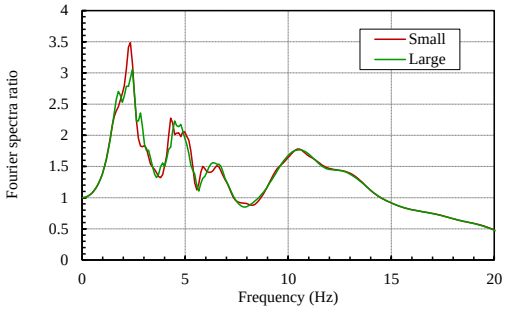

Fig. 9 Transfer function response

c) Difference between tetrahedral mesh and hexahedral mesh

In Section 4.1, a mesh based on tetrahedral elements was used because of its diagonal ground. However, in the finite element method, hexahedral elements (Fig. 10) are often used. Here, we will examine the differences between meshes with these elements. Figure 11 shows the analysis results where using tetrahedral element (Tetra10), which is a higher-order element, yielded almost the same results of a hexahedral element (Hex8).

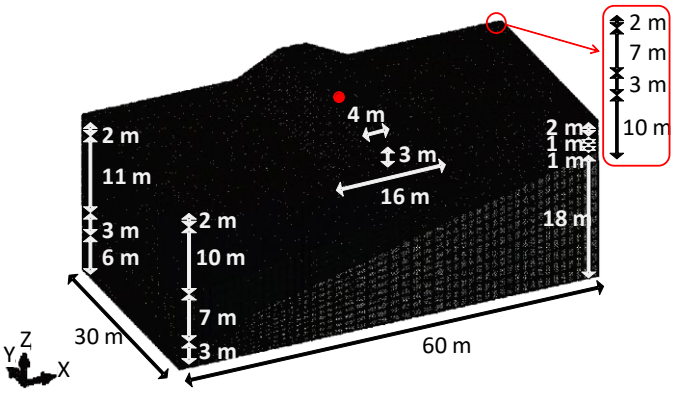

Fig. 10 Hexahedral element mesh

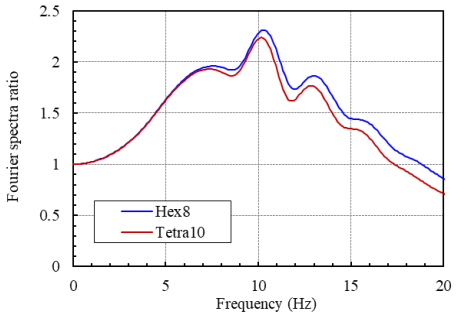

Fig. 11 Transfer function response of a mesh with tetrahedral (Teta10) and hexahedral (8) elements

5. Analysis results: Earthquake motion response

5.1 Analysis conditions

Liquefaction analysis using seismic motion was performed. The data in Table 1 is used for the ground properties. Sand layer 1 was used as the liquefied layer. Figure 12 shows the liquefaction strength curve in comparison with the data obtained by Toyoura sand. The soil constitutive equation used the YT model [4]. RL20 resistance strength is 0.2. Figure 13 shows the input ground motion of 2E.

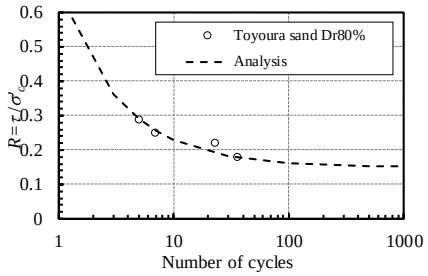

Fig. 12 Liquefaction strength curve

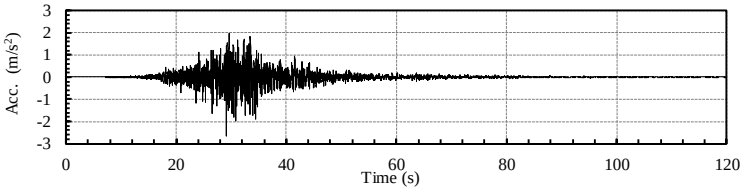

Fig. 13 Input ground motion

5.1 Analysis results

Figure 14 shows the Fourier spectrum ratio of the input acceleration and acceleration response applied with the Parzen window (0.2 Hz) at the center of the embankment top. A good response can be observed until 7 Hz. The largest difference can be observed around 8 Hz. Thus, if the ground liquefies, the frequency will be low and the effect of mesh difference is considerably small. Figure 15 shows the contour of the excess pore water pressure ratio of the central section of the mesh in Fig. 2(c) at 50 s where the shallower liquefied layer was completely liquefied.

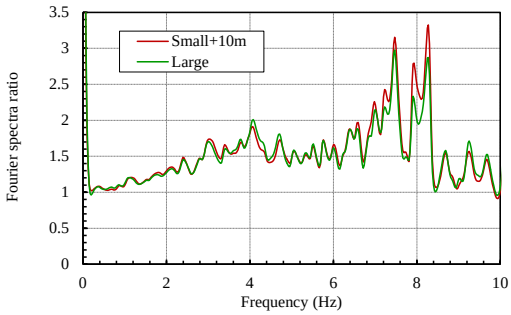

Fig. 14 Fourier spectrum ratio of the input acceleration and acceleration response

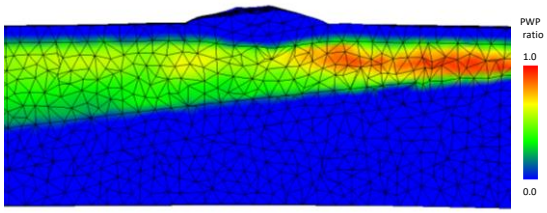

Fig. 15 Contour of excess pore water pressure ratio of the central mesh section at 50 s

6. Conclusion

In the study, the linear impulse response and transfer function of single-phase and the two-phase systems were analyzed. The seismic motion analysis of the two-phase system was also examined. Different boundary conditions were compared. The following findings were obtained:

1. When rigidly connecting the internal area and free field, accuracy deteriorates unless a sufficiently large mesh is set.

2. By adding the traction force, a similar response can be obtained from both large mesh and small mesh.

3. With irregular ground layer and free ground connected by a viscous boundary, the accuracy can be improved by setting the horizontal ground about 10 m from the irregular ground.

4. The analysis results for higher-order tetrahedral and hexahedral elements were almost the same.

5. Nonlinear liquefaction analysis showed similar results from a large mesh and a viscous boundary in a relatively small area.

7. References

[1] Lysmer, J. and Drake, L. (1972): A finite element method for seismology, Methods in Computational Physics 11,181–216.

[2] Fusanori M. and Hiroshi O. (1989): Dynamic analysis method for 3-D soil-structure interaction systems with the viscous boundary based on the principle of virtual work, Journal of JSCE, 404, 395–404. (in Japanese)

[3] Zienkiewicz, O. C. and Shiomi T. (1984): Dynamic behaviour of saturated porous media; the generalized Biot formulation and its numerical solution, International Journal for Numerical and Analytical Methods in Geomechanics 8.1, 71–96.

[4] Yoshida, H., Tokimatsu, K., Hijikata, K., Sugiyama, T., and Shiomi, T. (2008): Practical effective stress-strain model of sand considering cyclic mobility behavior, J. Struct. Constr. Eng., AIJ, 73(630), 1257–1264. (in Japanese)

